Earthquake Geotechnical Engineering for Protection and Development of Environment and Constructions – Silvestri & Moraci (Eds)
© 2019 Associazione Geotecnica Italiana, Rome, Italy, ISBN 978-0-367-14328-2

Ground motion amplification in the Zevulun Valley (Haifa Bay, Israel): Measurements and modeling

M. Tsesarsky & A. Goldberg
Ben Gurion University of the Negev, Israel

S. Shani-Kadmiel
Delft University of Technology, The Netherlands

O. Volk
University of Cambridge, UK

Z. Gvirtzman
Geological Survey of Israel, Jerusalem, Israel

ABSTRACT: The densely-populated Haifa Bay region is the main petrochemical hub of Israel. The seismic hazard of this area is elevated due to the proximity of active tectonic borders (Dead Sea Transform) and underlying sedimentary basin. Here we describe the results of two independent and complementing approaches to estimate ground motion amplification of this region. We report the results of seismic monitoring campaign using a transportable network deployed atop the sedimentary basin and adjacent rock site. We also report the results of a numeric wave propagation modeling using high-resolution geological model. Instrumental spectral ratios show that over the deepest parts of the sedimentary basin, and the location of main industrial hub, low frequency (< 1 Hz) amplification factors are up to a value of 8. Numerical amplification ratio maps of the entire region show comparable, to instrumental, amplification factors for low frequencies (< 0.75 Hz) and allow micro-zonation of seismic hazard of the Haifa Bay region.

1 INTRODUCTION

Measurements and damage observations of large earthquakes atop sedimentary basins have shown locally intensified ground motion (Aki and Larner 1970, Alex and Olsen 1998, Borcherdt 1970, Gao*, et al.* 1996, Graves*, et al.* 1998, Hartzell*, et al.* 2010, Trifunac and Udwadia 1974). Various methods for local basin-site response estimation have been introduced over time; Instrumental methods, rooted in measurement of seismic vibrations, provide ground motion amplification estimates by either comparing to a nearby reference-site where no amplification is expected, i.e., the traditional spectral ratio (SR) method (Borcherdt 1970) or by using the horizontal-to-vertical-spectral-ratio (HVSR) method at a single station (e.g. Nakamura 1989). Instrumental methods do not require prior knowledge of subsurface structure and lithology. However, they lack robustness, as local site effects can considerably change over short distances (Aki 1988).

The SR method requires simultaneous recordings of earthquake ground motions throughout basin- and reference-sites, a challenging task, especially in urban areas where anthropogenic noise limits the usable magnitudes and even more so in regions with moderate to low seismicity. On the other hand, HVSR methods rely on ambient vibrations and do not require recordings at reference-sites (e.g. Kagami*, et al.* 1982, Nakamura 1989). The theoretical basis of the method, however, is still debated as opposite explanations have been proposed and there is no simple correlation between H/V peak values and the actual site amplification factors (Bonnefoy-Claudet, *et al.* 2006). It is generally assumed that HVSR techniques predict the fundamental resonant frequency accurately, however, it is significantly less accurate in predicting amplification factors (Dravinski*, et al.* 1996, Huang 2002, Lachetl and Bard 1994, Mianshui*, et al.* 2017).

Many regions worldwide are known to be prone to seismic hazard, typically by established historic (pre-instrumental) records, but have little or no data of recorded earthquake ground motions. This may be due to limited deployment of seismic stations, long return periods, or a combination of the two.

1.1 *Seismic hazard of the Haifa Bay region*

The Zevulun Valley (ZV) is a deep and narrow basin underlying the Haifa Bay, a heavily populated and industrialized region, serving as the main petrochemical hub of Israel. It stretches along a 20-km coastline between the Carmel mountain in the south and the historical city of Acre in the north (Figure 1). Bound by the Mediterranean Sea in the west and the Galilee mountains foothills in the east, it is 9 km wide at its widest point. At the deepest point of the basin the hard carbonate rocks of the Judea Group, considered here as “basement”, are more than 1500 m deep. The ZV is in close proximity to active tectonic borders and potentially active faults. Within the basin, several reflectors of high impedance ratios are expected to amplify seismic ground motions.

Tectonic plate boundaries known as contributing factors to seismic hazard in the ZV are: the Dead Sea Transform (DST), less than 50 km away to the east and the Cyprus Arc, approximately 180 km to the north-west (Figure 1a). The DST is a left-lateral strike slip fault with low strain rate (4 - 5 mm/year), yielding low seismicity rate. Detailed pre-instrumental records of the Eastern Mediterranean dates back as far as 1200 BC (Agnon 2014) and includes numerous destructive earthquakes. The 1927 M 6.2 Jericho event was the last strong earthquake on the DST. It resulted in vast devastation and hundreds of casualties out of a total population of about 700,000 (British Palestine). This event predated the accelerated urban and industrial growth of the region in general, and the Haifa Bay area in particular. The subduction zone of the Cyprus Arc is capable of generating earthquakes with magnitudes > 6, with return periods of 50 years and > 7 with return periods of 500 years (Shapira and Hofstetter 2002).

In August 1984, M 5.3 earthquake occurred in the Jezreel Valley, about 10 km east of the Zevulun Valley. However, its relation to the Carmel Fault Zone (CFZ), which bounds the ZV in the south, is unclear. For seismic hazard analysis, the CFZ is assumed to generate earthquakes with magnitudes up to M 6.5 (Shamir*, et al.* 2001).

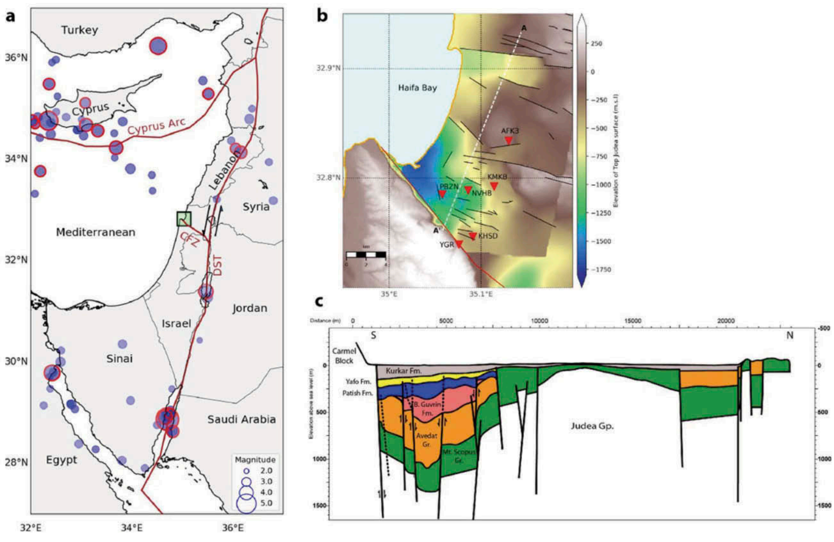

Figure 1. (a) Location map, tectonic borders and selected events (ZV net catalog) at the Eastern Mediterranean. The Haifa bay region is marked by a rectangle; (b) Elevation map of the top Judea reflector in the Haifa Bay area. Triangles indicate ZV net stations; (c) Longitudal (AA’) cross-section of the ZV.

1.2 *Ground motions amplification in the Haifa Bay*

Israel building code SI413, Design Provisions for Earthquake Resistance of Structures, (Israel Standards Institution 2013) addresses ground motion amplification via two basic inputs: a Vs30 based soil classification scheme for calculation of response spectra amplifications and a map of regions of potential high ground motion amplification. The map is a qualitative product, outlining such regions based on geological knowledge without quantitative output.

Ground motion amplification factors in the ZV were previously estimated using the HVSR technique by the Geophysical Institute of Israel (GII) in a coordinated effort led by Y. Zaslavsky (Zaslavsky*, et al.* 2006). Gvirtzman and Louie (2010) conducted a two-dimensional (2D) numerical study of ground motions atop of the ZV, which suggested that the deeper parts of the valley are likely to exhibit ground motion amplification factors in the order of 2 basin-wide with factors as high as 5 at local spots.

1.3 *Research goals*

In this paper, we introduce two independent data sets for estimating ground motion amplification at the Haifa Bay area. First, is spectral ratios of basin to reference sites based on simultaneous recordings of earthquakes during a 16 months' campaign of seismic monitoring with a transportable network consisting of 6 stations deployed in the Zevulun Valley. Second is ground motion amplification ratios computed using high-resolution 3-D geological model within a framework of a wave propagation numerical model (SW4).

The dataset contains first simultaneous earthquake ground motion recordings at basin- and reference-sites in Israel. We focus on a subset of 14 small and moderate earthquakes, $3 < Mw < 5.5$, at local and regional distances (Figure 1a), with the highest signal-to-noise ratio (SNR).

We begin with a structural description of the ZV geology, proceed with the estimation of measured and modeled ground motion amplification factors. Following we provide an interpretation of the recordings with regard to the deep geological structure of the basin. We conclude with a micro-zonation map of Peak Ground Velocity (PGV) amplification of the Haifa Bay region.

2 GEOLOGICAL STRUCTURE OF THE ZEVULUN VALLEY

The structural description of the ZV is based on a compilation of previous studies by Sagy and Gvirtzman (2009). The deep structure of the ZV is best visualized by the structural map of top Judea Gr. surface (Figure 1b) which is a significant regional reflector considered here as "basement". This surface reveals a steep, faulted relief buried under a sedimentary fill that forms the present flat topography (near MSL) of the valley. The ZV is a graben-horst-graben

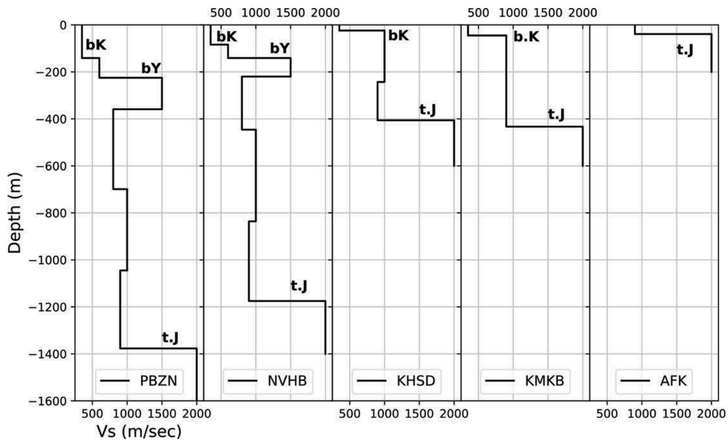

Figure 2. Velocity profiles of the ZV net stations.

structure forming two sub-basins separated by a flat rise. Bounded by east-west striking normal faults (Figure 1b), the southern graben is the Qishon graben (QG) and the northern graben is the Hilazon graben (HG). Separating them is the Afek Horst (AH). At its southern end, the valley is bounded by the seismically active Carmel fault zone. A longitudinal cross-section, (AA') through the ZV are presented in Figures 1c, illustrating that syn-tectonic units (the Bet Guvrin, Yafo and Patish Fm. of the Saqiye Gr.) thicken in the grabens and thins towards the Afek Horst. The Kurkar Gr. finally covers the entire ZV forming flat topography and leaving no expression for the horst-and-graben structure.

Sagy and Gvirtzman (2009) and Gvirtzman and Louie (2011) defined 6 structural reflectors for the ZV: (1) base of the Kurkar Gr. (Plio-Quaternary) - bK, (2) base of the Pliocene Yafo Fm. (laterally coinciding with the top of the Middle Miocene Ziqlag Fm., top of the Late Miocene Pattish Fm. - bY, (3) top Bet Guvrin Fm. (Oligocene-Miocene) - tBG, (4) base of the Saqiye Gr. (Late Eocene to Pliocene) - bSq, (5) top Mt Scopus Gr. (Late Cretaceous) - tMS, and (6) top Judea Gr. (Albian-Turonian)- tJ.

The Kurkar Gr. (Vs = 350 m/s) contains clayey and sandy soils, sand dunes, consolidated sandstones, conglomerates and unconsolidated sands. The underlying Yafo Fm. (Vs = 600 m/s) is composed of marls of shales. The Ziqlag/Patish formations (Vs = 1500 m/s) are composed of hard limestone. The Bet Guvrin formation (Vs = 800 m/s) is composed of marl. The Avedat Gr. (Vs = 1000 m/s) is composed of chalk and limestone. The Mount Scopus Gr. (Vs = 900 m/s) is composed of soft carbonates. Finally, at the bottom, the Judea Gr. (Vs = 2000 m/s) is composed of very hard limestone and dolomite with an impedance ratio of at least 2 with overlying formations.

3 THE ZV TRANSPORTABLE NETWORK

To study the earthquake-induced ground motions in the ZV the Geological Survey of Israel (GSI) deployed a transportable seismic network designed for shallow, quick installation and removal. Six stations were deployed for a period of 16 months (8/2014 to 12/2015) and maintained by the Geophysical Institute of Israel (GII). Deployment sites were chosen to sample different structural settings of the QG (Figure 1b) while considering practical limitations such as security of equipment and power supply, which contribute to anthropogenic noise. The seismometers were glued to a rock outcrop (YGR1 and KMKB), a concrete foundation (AFK3 and PBZN) or to fresh cement casting in a ~0.5 m deep pit (KHSD), and covered with a thermally insulating housing. The velocity profile under each station (Figure 2) was retrieved from the structural maps of major reflectors described Sagy and Gvirtzman (2009). Station YGR was installed on a hard rock outcrop (Judea Gr.) immediately south of the Carmel escarpment, attached to the Carmel block (Figure 1b). This station is the reference-site for other stations located on soft rocks within the basin.

3.1 *Data processing*

Raw data recorded during earthquakes was extracted from continuous recordings using the time stamp of the Israeli Seismic Catalog (published by the GII). These waveforms were demeaned, tapered with a 5% cosine taper, band-pass filtered between 0.1-10Hz and corrected for instrument response. In the case of the PBZN station (near the Haifa Bay Refineries), it was necessary to also apply a bandstop (notch) filter to in order to remove anthropogenic noise centered at 3 Hz. Station NVHB was bandpass filtered from 0.25 Hz to 10 Hz in order to avoid natural background noise at low frequencies.

Wave spectra were computed from the processed waveforms using 120 seconds' time windows covering the p and s waves windows of the record and smoothed using logarithmic smoothing function (Konno and Ohmachi 1998). For each station in the basin, spectral amplification ratios were computed relative to YGR1 and averaged over the selected events. SNR was computed for each station-event pair using the spectral approach (Bormann 1998) for 0.1 Hz - 1 Hz and 1 Hz -5 Hz windows. The higher frequency window was found to be significantly noisier

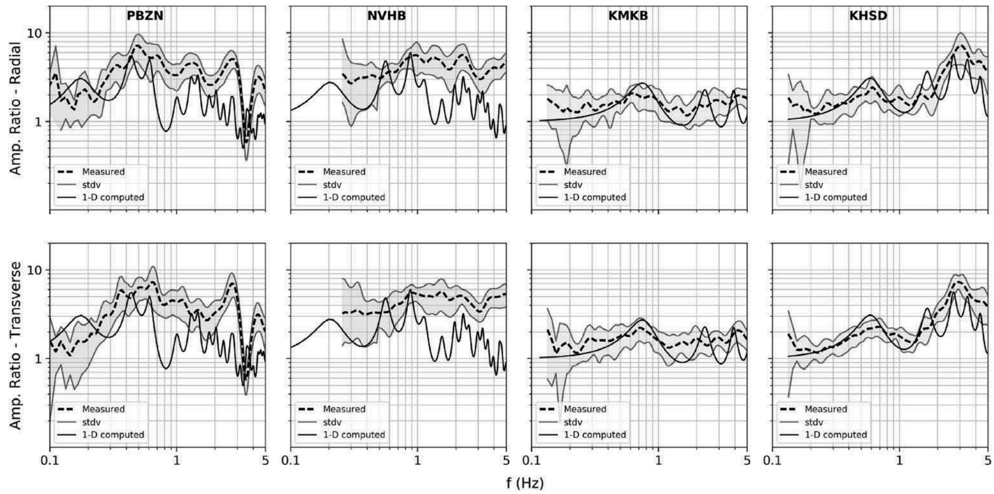

Figure 3. Spectral ground motion amplifications for the Radial component (upper panel) and Transverse component (lower panel) of the Zevulun Valley Network computed relative to YGR reference station, for earthquakes listed in Table 1. The dashed line is average instrumental value, the shaded area is one standard deviation from the average and the continuous line is 1-D linear elastic transfer function.

due to the strong anthropogenic noise in the region. However, SNR was typically above 4 and even at noisy stations like PBZN SNR at the 0.1 - 1 Hz band was above 10.

3.2 *Spectral amplification ratios*

Spectral amplification ratios (relative to reference station YGR) of the radial and transverse components for 15 earthquakes, $3 < M < 5.5$ (marked with red circle in Figure 1a) were averaged for stations PBZN, NVHB, KMKB and KHSD (Figure 3). The average spectral ratio is plotted using a dashed line, gray filling denotes one standard deviation (stdv) from average. For comparison, one-dimensional (1D) linear elastic transfer function corresponding to the velocity profile at each station is also plotted (solid line). This 1D transfer function was computed using the Strata software (Kottke and Rathje 2008). The linear elastic assumption was found to be appropriate for this case as the maximum shear strain of $5 \cdot 10^{-5}$ at the PBZN station (M 5.5 event) is near the non-linear strain threshold of 10^{-4} (Bereznev and Wen 1996, Kaklamanos*, et al.* 2015) and in most of the events reported here is about 10^{-6}.

4 NUMERICAL MODELING

The above-reported results are first of their kind for the Haifa Bay region. and provide valuable insights on ground motion amplification and seismic hazard in the region. However, these results apply only to five selected locations, with their respective limitations, over an area of about 200 km^2.To complement the measured amplification ratios and to cover the entire area of the Haifa bay we performed 3-D physics-based numerical analysis of seismic wave propagation.

4.1 *Model setup*

The six main reflectors of the ZV, as defined by Sagy and Gvirtzman (2009), were rasterized and incorporated into a regional velocity model of GII. The simulations domain is 85 km long, 104 km wide and 19 km deep. The horizontal dimensions were selected to accommodate the path to source effects, the epicentral location, finite source length and the boundary (supergrid) layers. The vertical dimensions were chosen to include the locking depth of the source (9 km) and the supergrid layer size.

Seismic wave propagation was modeled using the SW4 finite difference code (Petersson and Sjögreen 2015). The upper 6000 m of the model was discretized using 50 m grid spacing, lower parts were discretized with increasing grip spacing using the mesh refinement scheme embedded in SW4. The total number of grid points in the model was 453.10^6.

Based on recent geodetically constrained data (Hamiel*, et al.* 2016, Sadeh*, et al.* 2012) the Jordan Gorge Fault (JGF) and Kinnarot fault, north and south of the Sea of Galilee respectively, are locked, with slip deficit equivalent to M 7.1 and M 6.7 respectively. We modeled both fault scenarios, with M 6 earthquakes in order to quantify the ground motion amplification effects rather than focusing on specific PGV values. We employed the DSM finite fault model (Shani-Kadmiel*, et al.* 2016) developed and validated by our research group. We assumed northward directivity of the rupture. A Gaussian velocity-time function with a fundamental frequency of $f_0 = 0.33$ Hz and maximal frequency of $f_{max} = 0.75$ Hz was prescribed to the source.

4.2 *Simulations results*

In what follows we focus on the amplification ratio of the two source scenarios. As site effect is mostly source-path independent we will focus on the Kinnarot (KNR) fault scenario. PGV map of the KNR scenario is presented in Figure 4 alongside a PGV map of latterly homogenous (regional velocity model) reference model. The prominent ground motion amplification atop the ZV structure is clearly visible. The PGV values over the deeper parts of the basin are of the same magnitude as in the source near-field area, although the epicentral distance to the QG is 54 km. Clearly, both grabens of the ZV amplify ground motions, with stronger amplification over the QG at the southern part of the ZV. The amplification over the QG can be attributed to several effects, including deeper structure, soft syn-tectonic units fully represented and the edge effect by the Carmel Fault.

Dividing the basin PGV map by the reference PGV map yields the amplification (AF) factor map, presented in Figure 5a. The AF reaches a maximum value of 10 atop the deepest part of the QG, and typically exceeds the value of 4 over the southern part. Amplification factors atop the northern part of the ZV (the HG) are lower than 4, as expected due its shallower structure and absence of soft syn-tectonic sediments of the ZV. Examination of the synthetic seismogram for the location of station PBZN (Figure 5b) and its spectral ratios (where H/H is relative to YGR reference station) shows two amplification peaks at 0.2 Hz with a magnitude of 9 (y component), and at 0.5 Hz with a magnitude of 6 (x component). These amplification peaks are at similar frequencies to ones measured at station PBZN. Given that our source is

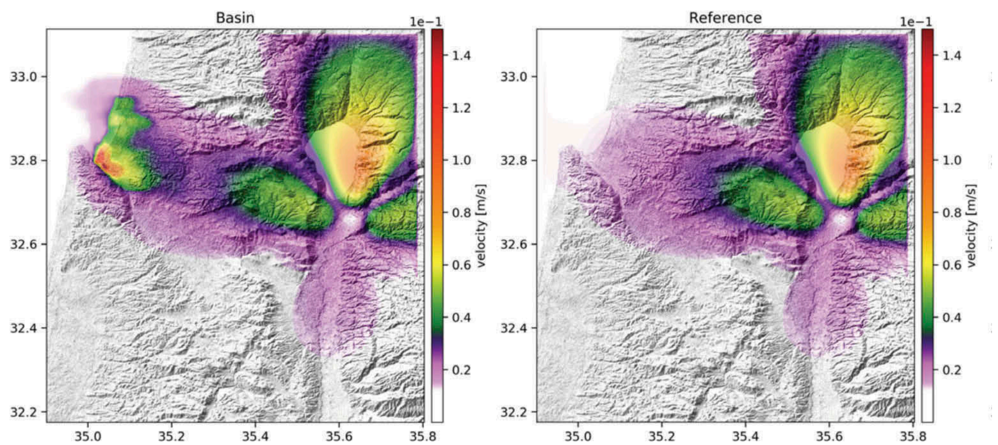

Figure 4. Peak Ground velocity maps of KNR source scenario: basin model (left) model and reference model (right).

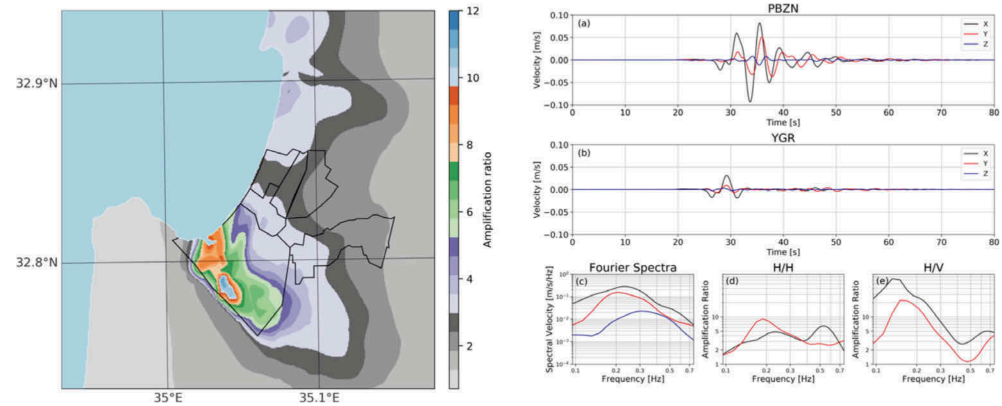

Figure 5. (a) Amplification map of the Haifa bay region (left) and (b) synthetic seismogram and spectral rations for the locations of station PBZN and YGR (right).

limited to low frequencies (< 0.75 Hz) ground amplification at higher frequency (e.g. over the AH and HG) is not captured by our model, and the map presented in Figure 5a is a low-frequency amplification map.

5 CONCLUSIONS

In this paper, we study ground motion amplification of the Haifa Bay region. The region is found in proximity to active tectonic borders and is underlain by a deep sedimentary basin. The tectonic setting, geological structure and mixed land use, including petrochemical works in dense urban setting, significantly increase the seismic hazard and risk of the region.

We computed ground motion spectral ratios and amplification factors using simultaneous measurements of earthquakes on basin and rock sites, using a transportable network of six broadband seismometers deployed over a period of 16 months. Independently we computed PGV and ground motion amplification maps via numerical modeling of seismic wave propagation using high-resolution geological model and different source scenarios.

Both measured and calculated amplification factors show high ground motion amplification atop the deepest parts of the sedimentary basin. Instrumental, low frequency (< 1 Hz) amplification ratios are up to a factor of 8 (average value) with distinct peaks for deep and shallow regional reflectors. Shallower regions of the basin exhibit amplifications at higher frequencies of lower magnitude.

Numerical amplification ratios for comparable locations and low frequencies (< 0.75) show similar amplification peaks. The 50 m resolution of the numerical model results in a detailed micro-zonation map, which complements the sparse instrumental coverage.

REFERENCES

Agnon, A. (2014). Pre-Instrumental Earthquakes Along the Dead Sea Rift, in *Dead Sea Transform Fault System: Reviews* Z. Garfunkel, Z. Ben-Avraham and E. Kagan (Editors), Springer, 207-262.

Aki, K. (1988). Local Site Effects on Strong Ground Motion, in *Earthquake Engineering and Soil Dynamics II—Recent Advances in Ground-Motion Evaluation* J. L. Von Thun (Editor), ASCE, 103-155.

Aki, K., and K. L. Larner (1970). Surface Motion of a Layered Medium Having an Irregular Interface Due to Incident Plane SH Waves, *J. Geophys. Res*. **75** 933-954.

Alex, C. M., and K. B. Olsen (1998). Lens effect in Santa Monica?, *Geophys. Res. Lett*. **25** 3441-3444.

Bereznev, I. A., and K. Wen (1996). Nonlinear soil response—A reality?, *Bulletin of the Seismological Society of America* **86** 1964-1978.

Bonnefoy-Claudet, S., F. Cotton, and P.-Y. Bard (2006). The nature of noise wavefield and its applications for site effects studies A literature review, *Earth Science Reviews* **79** 205-227.

Borcherdt, R. D. (1970). Effects of local geology on ground motion near San Francisco Bay, *Bulletin of the Seismological Society of America* **60** 29-61.
Dravinski, M., G. Ding, and K.-L. Wen (1996). Analysis of spectral ratios for estimating ground motion in deep basins, *Bulletin of the Seismological Society of America* **86** 646-654.
Gao, S., H. Liu, P. M. Davis, and L. Knopoff (1996). Localized amplification of seismic waves and correlation with damage due to the Northridge earthquake: Evidence for focusing in Santa Monica, *Bulletin of the Seismological Society of America* **86** S209-230.
Graves, R. W., A. Pitarka, and P. G. Somerville (1998). Ground-motion amplification in the Santa Monica area: Effects of shallow basin-edge structure, *Bulletin of the Seismological Society of America* **88** 1224-1242.
Gvirtzman, Z., and J. N. Louie (2010). 2D Analysis of Earthquake Ground Motion in Haifa Bay, Israel, *Bulletin of the Seismological Society of America* **100** 733-750.
Gvirtzman, Z., I. Makowski, and Y. Sagee (2011). Re-processing and geological re-interpretation of old seismic lines of Haifa bay, Geological Survey of Israel.
Hamiel, Y., O. Piatibratova, and Y. Mizrahi (2016). Creep along the northern Jordan Valley section of the Dead Sea Fault, *Geophysical Research Letters* **43** 2494-2501.
Hartzell, S., L. Ramirez-Guzman, D. Carver, and P. Liu (2010). Short Baseline Variations in Site Response and Wave-Propagation Effects and Their Structural Causes: Four Examples in and around the Santa Clara Valley, California, *Bulletin of the Seismological Society of America* **100** 2264-2286.
Huang, H.-C. (2002). Characteristics of earthquake ground motions and the H/V of microtremors in the southwestern part of Taiwan, *Earthquake Engineering & Structural Dynamics* **31** 1815-1829.
Israel Standards Institution (2013). Standard SI 413. Design Provisions for Earthquake Resistance of Structures. Amendment No. 5.
Kagami, H., C. M. Duke, G. C. Liang, and Y. Ohta (1982). Observation of 1- to 5-second microtremors and their application to earthquake engineering. Part II. Evaluation of site effect upon seismic wave amplification due to extremely deep soil deposits, *Bulletin of the Seismological Society of America* **72** 987-998.
Kaklamanos, J., L. G. Baise, E. M. Thompson, and L. Dorfmann (2015). Comparison of 1D linear, equivalent-linear, and nonlinear site response models at six KiK-net validation sites, *Soil Dynamics and Earthquake Engineering* **69** 207-219.
Kottke, A., and E. M. Rathje (2008). A Semi-Automated Procedure for Selecting and Scaling Recorded Earthquake Motions for Dynamic Analysis, *Earthquake Spectra* **24** 911-932.
Lachetl, C., and P. Bard (1994). Numerical and Theoretical Investigations on the Possibilities and Limitations of Nakamura's Technique, *Journal of Physics of the Earth* **42** 377-397
Mianshui, R., L. Y. Fu, Z. Wang, X. Li, N. S. Carpenter, E. W. Woolery, and Y. Lyu (2017). On the Amplitude Discrepancy of HVSR and Site Amplification from Strong-Motion Observations, *Bulletin of the Seismological Society of America* **107** 2873-2884.
Nakamura, Y. (1989). A Method for Dynamic Characteristics Estimation of Subsurface using Microtremor on the Ground Surface, in *Quarterly Report of Railway Technical Research Institute (RTRI)*,.
Petersson, N. A., and B. Sjögreen (2015). Wave propagation in anisotropic elastic materials and curvilinear coordinates using a summation-by-parts finite difference method, *J. Comput. Phys*. **299** 820-841.
Sadeh, M., Y. Hamiel, A. Ziv, Y. Bock, P. Fang, and S. Wdowinski (2012). Crustal deformation along the Dead Sea Transform and the Carmel Fault inferred from 12 years of GPS measurements, *J. Geophys. Res*. **117** B08410.
Sagy, Y., and G. Gvirtzman (2009). Subsurface mapping of the Zevulun Valley (Hebrew), The Geophysical Institute of Israel, Report 648/454/09.
Shamir, G., Y. Bartov, A. Sneh, L. Fleischer, V. Arad, and M. Rosensaft (2001). Preliminary seismic zonation for Israel. GII Rept. No. 550/95/01(1).
Shani-Kadmiel, S., Z. Gvirtzman, and M. Tsesarsky (2016). Distributed Slip Model for Forward Modeling Strong Earthquakes, *Bulletin of the Seismological Society of America* 106.
Shapira, A., and A. Hofstetter (2002). Seismicity Parameters of Seismogenic Zones, Geophysical Institute of Israel. Report Num. 592/230/02, 74pp.
Trifunac, M. D., and F. E. Udwadia (1974). Variations of strong earthquake ground shaking in the Los Angeles area, *Bulletin of the Seismological Society of America* **64** 1429-1454.
Zaslavsky, Y., T. Akseinko, M. Gorstein, A. Hofstetter, M. Kalmanovich, N. Perelman, V. Giller, D. Livshits, D. Giller, G. Ataev, I. Dan, and A. Shvartsburg (2006). Empirical determinations of local site effect using ambient vibration measurements for the earthquake hazard and risk assessment to Qrayot-Haifa Bay areas, Geophysical Institute of Israel. Report Num. 595/064/06.